Resilient Microgrid Energy Management Algorithm Based on Distributed Optimization

Vittorio Casagrande, Ionela Prodan, Sarah K. Spurgeon, *Fellow, IEEE*, and Francesca Boem, *Member, IEEE*

***Abstract*—This article proposes a fully distributed energy management algorithm for dc microgrids, resilient to different faults. Specifically, we employ distributed model-predictive control to deal with the uncertainty that characterizes the microgrid operation. The optimization problem is solved at each time step through a distributed optimization algorithm, which has three main advantages: 1) agents of the network require a small computational power; 2) local information is not shared among the network nodes, hence preserving a certain level of privacy; and 3) it is suitable for implementation in large-scale systems. The resilience property of the algorithm stems from additional constraints that are enforced in order to store in the system enough energy to sustain the microgrid in the case of utility grid or line fault. Simulation results show that the algorithm is suitable to schedule the operation of agents that are always connected to the microgrid (e.g., loads) as well as agents that may be connected and disconnected (e.g., electric vehicles).**

***Index Terms*—Distributed control, distributed optimization (DO), energy management, microgrid, model-predictive control (MPC).**

NOMENCLATURE

$P_{r,i}$	ith renewable generator power.
$P_{r,i}^M$	Max power of the ith renewable generator.
$P_{l,i}$	ith load power.
d_i^M d_i^m	Max, min power demand of the ith load.
$P_{s,i}$	ith storage system power.
$P_{s,i}^M$	Max power of the ith storage system.
$P_{z,i}$	ith electric vehicle power.
$P_{z,i}^M$	Max power of the ith electric vehicle.
$P_{g,i}$	ith external tie power.
$P_{g,i}^M$ $P_{g,i}^m$	Max, min power of the ith external tie.
s_i	ith storage charge.
s_i^M s_i^m	Max, min charge of the ith storage.
z_i	ith electric vehicle charge.
z_i^M z_i^m	Max, min charge of the ith electric vehicle.
z_i^*	Target battery charge of the ith electric vehicle.
$\mu_{i,c/d}$	Energy conversion efficiency of the ith storage related to charging $\mu_{i,c} < 1$ or discharging $\mu_{i,d} > 1$.
$\eta_{i,c/d}$	Energy conversion efficiency of the ith electric vehicle related to charging $\eta_{i,c} < 1$ or discharging $\eta_{i,d} > 1$.
$P_{B,i}$	Power injection in bus i.
$P_{L,i}$	Power flowing through line i.
$P_{L,i}^M$	Max power flowing through line i.
$J_{*,i}$	Objective function of the ith agent of type $*$, where $* \in \{r, l, s, z, g\}$ (renewable generator, load, storage, electric vehicle, and external tie).
$w_{*,i}$	Objective function weight of the ith agent of type $*$, where $* \in \{r, l\}$ (renewable generator, load), $* \in \{s, z\}$ (storage, electric vehicle), and $* \in \{P_{s,i}, P_{z,i}\}$ (associated with storage, electric vehicle power).
p_g	Electricity price.
N_*	For $* \in \{r, l, s, z, g, B, L\}$, number of renewable generators, loads, storages, electric vehicles, external ties, buses, and lines.
$\tilde{N}_z$	Subset of vehicles provided with V2G technology.
$t_{L,j}^i$ $t_{L,j}^f$	Initial, final time of the fault at line j.
t_g^i t_g^f	Initial, final time of the distribution grid fault.
τ_i^i τ_i^f	Time when the electric vehicle is plugged, unplugged.
$\tilde{r}_\nu$	Minimum load energy requirement for the next ν steps.
T_s	Sample time of the controller.
T	Time horizon of the controller.
ε_i	Optimization variable used to soften the constraint on the minimum storage charge.
λ_i	Weight associated with the variable ε_i.

Manuscript received 7 March 2022; revised 17 July 2022; accepted 7 October 2022. This work was supported in part by the PHC Alliance Hubert Curien Programme under Grant 43234RH and in part by the University College London Engineering and Physical Sciences Research Council under Grant EP/R513143/1. The work of I. Prodan's supported by FMJH Program PGMO and in part by EDF. *(Corresponding author: Vittorio Casagrande.)*

Vittorio Casagrande, Sarah K. Spurgeon, and Francesca Boem are with the Department of Electronic and Electrical Engineering, University College London, London WC1E 6BT, U.K. (e-mail: vittorio.casagrande.19@ucl.ac.uk; s.spurgeon@ucl.ac.uk; f.boem@ucl.ac.uk).

Ionela Prodan is with the University Grenoble Alpe, Grenoble INP†, 26000 Valence, France (e-mail: ionela.prodan@lcis.grenoble-inp.fr).

Digital Object Identifier 10.1109/JSYST.2022.3216205

†Institute of Engineering and Management University Grenoble Alpes.

I. INTRODUCTION

MICROGRID systems, first introduced in [1], are defined as clusters of loads, distributed generation units, and energy storage systems, operated in coordination to reliably supply electricity and connected to the power distribution grid [2]. Typically, the control of a microgrid system is deployed in three layers [3].

1) The primary control layer is in charge of voltage and frequency regulation.
2) The secondary layer deals with power quality issues.

3) The tertiary layer is responsible for power flow control, power management, and optimization of the microgrid operation.

As a part of the tertiary control layer, the energy management system (EMS) is the controller that computes the power flows in order to provide a stable delivery of power to loads while optimizing energy production and other operational goals [4]. As described in [5], the main challenges in the design of the microgrid EMS are the uncertainty that characterizes renewable power production and load consumption, privacy-related issues, and resilience to faults in the infrastructure. While the first problem has been well addressed in the literature, a few papers focus on the last two. In particular, privacy issues are becoming increasingly important [6]: sharing the load demand profile can reveal details of a manufacturing process or of the distribution system operator controllers making the system prone to cyber-attacks.

In this article, we propose an EMS that guarantees a certain level of resiliency while keeping local information private. To do this, we design a distributed controller architecture based on distributed optimization (DO) and model-predictive control (MPC). The distributed formulation of the problem allows the controller to schedule the operation of all the components connected to the microgrid while keeping all local information private. Moreover, as opposed to centralized architectures, the algorithm is easily scalable to large-scale systems (LSSs), relies only on neighbor-to-neighbor communication, and requires a small amount of computational power. Finally, the EMS algorithm is suitable for the wide range of agents that can be connected to the microgrid, from renewable power generators to electric vehicles (EVs).

A. Literature Review

1) Handling Uncertainties: Since the first introduction of the microgrid concept, many EMSs have been proposed in the literature to schedule the microgrid operation for one step ahead, e.g., [7], where time steps further away in the future are not considered, or for longer periods, e.g., [8], where the schedule is computed for the next 24 h without considering the uncertainty that affects the system. MPC-based methods have proved their effectiveness for the EMS application since the optimization problem is reformulated at each time step, hence compensating for uncertainty. In particular, centralized MPC has been used to schedule the power profile of storage devices [9], controllable generators, controllable loads, connection to the utility grid [10], and EVs [11]. All these methods aim at optimizing the microgrid operation, penalizing either repeated charges or discharges of the batteries [9], repeated turn ON and OFF of generators [10], and maximizing the revenue from energy selling [11]. In order to compute less conservative control actions when the probability distribution of uncertainty is available, stochastic MPC algorithms can be designed. For example, in [12], the optimization problem is formulated as a chance-constrained problem, whereas, in [13], a scenario-based approach is employed. The EMS design gets more complex if the presence of EVs is explicitly considered. Undoubtedly, EV integration gives several advantages [14]; however, owing to their high energy demand, suitable control algorithms need to be designed [15]. A power management method that integrates the objectives and constraints of EVs with the other microgrid components (e.g., households and storage units) has been proposed in [16] for the centralized case.

2) Distributed EMS: Although all the aforementioned methods are suitable for uncertainty compensation, they do not take into account privacy-related issues and potential fault effects. Distributed methods have been proposed to overcome the limitations of centralized MPC, in particular regarding the computing power and privacy issues [17]. In [18], each component (e.g., gas turbine or battery) solves a local MPC problem and coordinates with the other agents exchanging power profiles to optimize the global performance. In [19] and [20], a distributed MPC method is proposed to solve the energy management problem for multiple microgrids and a large-scale power system. However, both methods rely on a central unit for coordination, hence being subject to limitations of centralized approaches and require to share local data. A fully distributed EMS that keeps private local data is proposed in [21], where a DO-based MPC algorithm is proposed. The main drawback of this method is that the microgrid topology is not considered as well as possible faults.

3) Resilient EMS: The microgrid itself offers advantages in terms of system resiliency to faults being provided with local generation units and storage systems that allow it to be operated in the island mode (i.e., disconnected from the utility grid) [22]. There are mainly three strategies that can be implemented to enhance the microgrid resilience [23]: 1) fault detection; 2) proactive scheduling; and 3) outage management. We do not deal with the first strategy since this operation is often performed at lower control layers; however, we implement both the other two in our algorithm. By *proactive scheduling*, we mean that the system is prepared for potential fault events before their occurrence by scheduling the resources in a conservative way. By *outage management*, we mean adapting the controller objectives and constraints in order to assure the critical power demand to loads. Even though the literature on energy management is extensive, few papers propose resilient algorithms for EMS, and to the best of the authors knowledge, none of them is distributed. On the one hand, only reconfiguration strategies once the fault has occurred are proposed in the literature. Outage management approaches are proposed in [24] using MPC and in [25] using reinforcement learning for the home EMS. The objectives are to deliver energy to critical loads while minimizing the power curtailment to other loads. Such methods, however, do not ensure power delivery to critical loads for persistent faults. Controller reconfiguration strategies are proposed to deal with faults in microgrid systems [26] and industrial plants [27], in which there are many backup options to generate the required amount of power; hence, storing an amount of backup energy may not be necessary. On the other hand, many papers propose proactive scheduling methods to deal with faults. A common approach is to ensure the power delivery to loads by storing an additional fixed amount of energy in the storage systems (typically 20–30% of the capacity) to be used in the case of utility grid fault without taking into account the future load demand [28], [29]. In [30], the amount of backup energy is adapted to the minimum future

power requirement of the loads, and in [31], it is computed by solving an optimization problem. The drawback of such methods is that they require to share with the centralized controller all the future loads' demands. Finally, a number of papers propose to use the energy stored in EVs to supply the loads during power outages [32], [33]. However, these papers assume that EVs are connected to the microgrid and that they have enough energy during the whole fault duration.

B. Contributions

This article presents a DO-based MPC algorithm for energy management that guarantees the privacy of local information. Preliminary results have been presented in [34]. In particular, we design the EMS as an MPC controller in which the optimization problem is solved using a DO algorithm that allows all the local information of each agent to be kept private. Here, in addition, we consider the possible occurrence of faults in the microgrid system, and we implement proactive scheduling and outage management strategies. As a proactive scheduling strategy, in order to ensure the delivery of power to loads during faults, we propose to store a variable amount of backup energy in batteries and EVs. The amount of backup energy is adapted to the future power demand of loads so that the storage capacity that is not devoted to fault tolerance can be used for typical purposes of an EMS (e.g., peak shaving/valley filling). Finally, since the duration of a fault is not known in advance, we allow the battery to be fully drained if necessary by introducing a soft constraint on the minimum state of charge (SoC). Our algorithm is suitable to integrate different types of agents that are connected to the microgrid. In particular, it is suitable to schedule the charging of EVs that are temporarily connected to the microgrid considering the plugging and unplugging events as additional constraints within the optimization problem. To summarize, the main novel contributions of the designed EMS are as follows.

1) It is fully distributed, requires a small computational power for each agent, and keeps all local information private.
2) It is resilient to faults, meaning that it allows the delivery of power to loads under different fault conditions (such as utility grid fault).
3) It integrates the objectives and constraints of EVs to those of other agents, potentially using their storage capacity to increase resilience.
4) It can be easily extended to LSSs.

The rest of this article is organized as follows. In Section II, the models of each microgrid component and possible faults are presented. In Section III, the proposed EMS is described. In Section IV, extensive simulation results are provided. Finally, Section V concludes this article.

II. System Model

In this section, we present the model of the microgrid and describe the communication network required to implement the proposed distributed control architecture. We conclude by introducing the model of the possible microgrid faults.

A. Microgrid

The microgrid is composed of five agents: renewable generators, loads, storage systems, EVs, and utility grid connections. The model presented in this section builds upon the model developed in [34] with the addition of EVs and fault models.

1) Renewable Generators: Renewable generators, such as wind generators and photovoltaic (PV) panels, produce power to be injected in the microgrid. The amount of power that can be injected in the grid is limited by the maximum power produced by the renewable generator

$$0 \leq P_{r,i}(t) \leq P^M_{r,i}(t). \tag{1}$$

Their objective is to maximize the power that they inject in the grid; hence, the associated objective function is written as

$$J_{r,i}(t) = \sum_{k=0}^{T-1} \gamma^k w_{r,i} \left[P_{r,i}(t+k) - P^M_{r,i}(t+k)\right]^2 \tag{2}$$

where $\gamma \in [0;1]$ is used to reduce progressively the importance of time steps further away in the future (hence more uncertain).

2) Loads: Loads include all the consumers that can only draw energy from the microgrid, e.g., households and factories. Each load is characterized by a maximum and a minimum power demand

$$d^m_i(t) \leq P_{l,i}(t) \leq d^M_i(t) \tag{3}$$

where d^m_i is the critical power demand that must be met. Loads maximize the power that they draw from the grid (without exceeding the upper limit); hence, their objective function is

$$J_{l,i}(t) = \sum_{k=0}^{T-1} w_{l,i} \left[P_{l,i}(t+k) - d^M_i(t+k)\right]^2. \tag{4}$$

3) Storage Systems: Storage systems are installed in microgrids to assist the renewable power integration by compensating for intermittence and preventing load fluctuations [35]. There are many other advantages obtained from installing energy storage systems in a microgrid, e.g., power quality, frequency regulation, and black start [36], [37]. Depending on the specific goal, a different storage system model has to be used. Since, in this article, we are interested in the energy management problem (peak shaving and renewable energy shifting), we do not need a particular model for each specific storage technology; hence, we model it as a first-order linear system as in [10] and [30]

$$s_i(t+1) = s_i(t) + \mu_{i,c/d} T_s P_{s,i}(t). \tag{5}$$

The energy conversion efficiency is typically 90–95% of the exchanged energy [10] ($\mu_{i,c} < 1$ and $\mu_{i,d} > 1$). The maximum and minimum amount of energy, which can be stored in the storage, are denoted by s^m_i and s^M_i:

$$s^m_i \leq s_i(t) \leq s^M_i. \tag{6}$$

There are many factors that affect the lifetime of a storage system, mainly the depth of discharge and the discharging rate [38], [39]. To increase the battery lifetime and avoid the rapid degradation of its performances, the lower limit of charge is typically higher than zero (the usable energy is between 80% and 95% of the total energy). The power exchanged with the grid is limited by a maximum value

$$-P^M_{s,i} \leq P_{s,i}(t) \leq P^M_{s,i}. \tag{7}$$

Power is assumed to be negative when it is injected in the microgrid, consistently with (5). The objectives of the storage system agent are expressed as a quadratic function of stored energy and exchanged power

$$J_{s,i}(t) = \sum_{t=0}^{T-1} w_{P_s,i} \left[P_{s,i}(t) - \bar{P}_{s,i}(t)\right]^2 + w_{s,i} \left[s_i(t) - \bar{s}_i(t)\right]^2 \tag{8}$$

where $\bar{P}_{s,i}(t)$ and $\bar{s}_i(t)$ are target values that are set to meet the control objectives; for example, if we need to penalize the battery usage to increase its lifetime, we set $\bar{P}_{s,i}(t)$ to zero.

4) Electric Vehicles: A wide range of EVs are on the market; most of them either run solely on electric propulsion (battery EVs) or they may have an internal combustion engine working alongside (hybrid EVs). The energy for electric propulsion is stored in a battery that is modeled as a first-order system

$$z_i(t+1) = z_i(t) + \eta_{i,c/d} T_s P_{z,i}(t). \tag{9}$$

The energy conversion efficiency is typically 90–95% of the exchanged energy [40] ($\eta_{i,c} < 1$ and $\eta_{i,d} > 1$). The amount of energy that can be stored in the battery is limited by a maximum and a minimum value, so that

$$z_i^m \leq z_i(t) \leq z_i^M. \tag{10}$$

As for the case of batteries, the lower limit of charge is higher than zero to increase the battery lifetime. Typically, the usable energy is between 80% and 95% of the total energy [41]. The power that can be exchanged with the grid is limited

$$P_{z,i}^m \leq P_{z,i}(t) \leq P_{z,i}^M. \tag{11}$$

The power exchanged with the grid can be unidirectional or bidirectional depending on the vehicle [14]. In the first case, the lower power limit is set to zero ($P_{z,i}^m = 0$), whereas in the second case (vehicle-to-grid (V2G) technology), the lower power limit is $P_{z,i}^m = -P_{z,i}^M$. In contrast to other storage systems connected to the microgrid, EVs, although being parked up to 90% of their time [42], may be plugged or unplugged, and it may not be possible to absorb their energy if the microgrid requires it due to the driver's necessities. Typically, the EV will be parked for a certain amount of time, at the end of which a predefined SoC has to be reached. This is modeled through a constraint on the final SoC of the battery

$$z_i(\tau_i^f) \geq z_i^*. \tag{12}$$

Similarly to storage systems, the objective function of an EV is written in terms of power and SoC

$$J_{z_i} = \sum_{t=0}^{T-1} w_{P_{z,i}} \left[P_{z,i}(t) - \bar{P}_{z,i}(t)\right]^2 + w_{z,i} \left[z_i(t) - \bar{z}_i(t)\right]^2 \tag{13}$$

where $\bar{P}_{z,i}(t)$ and $\bar{z}_i(t)$ are target values.

5) External Connections: Microgrids are connected to the utility grid at one or more points, and the power $P_{g,i}$ that can be exchanged with it is limited by a maximum value

$$P_{g,i}^m \leq P_{g,i}(t) \leq P_{g,i}^M. \tag{14}$$

The goal of the external connection agent is to minimize the total energy cost (maximize the energy that is sold and minimize the energy that is bought); hence, its objective function can be formulated as

$$J_{g,i} = -\sum_{t=0}^{T-1} p_g(t) P_{g_i}(t). \tag{15}$$

The power sign is assumed positive when energy is sold to the utility grid; hence, the minus sign is introduced to penalize buying and encourage selling.

6) Buses and Lines: The interconnection of the agents is realized through buses and lines; in particular, each component of the microgrid is connected to a bus, and buses are connected through lines; hence, these interconnections represent additional constraints of the EMS [13], [43]. The first constraint is the power balance, that is, the sum of the powers exchanged with each bus has to be equal to zero

$$\sum_{i=1}^{N_B} P_{B,i} = 0. \tag{16}$$

The second constraint is given by the maximum line power flow; namely, the maximum power flowing through each line is limited by its maximum value

$$-P_{L,i}^M \leq P_{L,i}(t) \leq P_{L,i}^M. \tag{17}$$

The dc power flow equation is used to compute $P_{L,i}$ [44]

$$\mathbf{P}_L(t) = \mathbf{b}\mathbf{A}_B^L \mathbf{B}^{-1} \mathbf{P}_B(t) \tag{18}$$

where $\mathbf{P}_L \in \mathbb{R}^{N_L}$ is a vector obtained stacking line power flows, $\mathbf{b} \in \mathbb{R}^{N_L \times N_L}$ is a diagonal matrix in which each element $b(i,i)$ is the susceptance of line i, $\mathbf{B} \in \mathbb{R}^{N_B \times N_B}$ is the admittance matrix, and $\mathbf{P}_B \in \mathbb{R}^{N_B}$ is the vector obtained stacking all the bus injections $P_{B,i}$. The elements of the microgrid adjacency matrix $\mathbf{A}_B^L \in \mathbb{R}^{N_L \times N_B}$ are $A_B^L(i,j) \in \{0, 1, -1\}$, respectively, if line i and bus j are not connected, line i starts at bus j, or line i ends at bus j.

B. Communication Network

The communication network allows the agents to coordinate their activity. In particular, the EMS is implemented as a distributed MPC, where a communication network is required to solve a DO problem. The communication network is represented by an undirected graph $G(\mathcal{V}, \mathcal{E})$, where $\mathcal{V}$ is the set of nodes and $\mathcal{E}$ is the set of edges. Each node corresponds to an agent of the microgrid associated with a microgrid component (e.g., load or EV); hence, the total number of agents is

$$N = N_r + N_l + N_s + N_z + N_g. \tag{19}$$

The total number of agents is equal to the cardinality of the set $\mathcal{V}$, $N = |\mathcal{V}|$. The communication graph at time t is represented by its adjacency matrix $A(t) \in \mathbb{R}^{N \times N}$, where $a_{i,j} = 1$ if the components i and j are connected and $a_{i,j} = 0$ otherwise. It should be noted that the communication network may differ from the physical interconnection, i.e., two nodes that are not interconnected through a power line may exchange data. Nodes that can communicate are denoted as neighbors.

C. Fault Models

There are three types of faults that are relevant for the EMS:

1) line fault;
2) distribution grid fault;
3) communication network fault.

1) Line Faults: When a line fault occurs, power can no longer flow through the faulty line. In the EMS, this is modeled by modifying constraint (17). The power that flows through the faulty line (j in this case) is set to zero from $t^i_{L,j}$ to $t^f_{L,j}$:

$$P_{L_j}(t) = 0 \quad \forall t \in \left[t^i_{L,j}, t^f_{L,j}\right]. \tag{20}$$

If the fault duration is known in advance, this constraint is enforced only until recovery. On the contrary, if the fault duration is not known, the constraint is enforced for all future time steps. As a consequence of a line fault, power has to flow through the other lines at the risk of line overloading. It is clear that this applies only to meshed microgrids; if a line fault occurs in a radial microgrid, there is no way to deliver power to the disconnected microgrid branch.

2) Distribution Grid Fault: In this case, the microgrid cannot draw power from the utility grid until recovery. This is modeled by modifying constraint (14) as follows:

$$P_{g,i}(t) = 0 \quad \forall\, i \in \{1 \dots N_g\} \ \forall t \in \left[t^i_g, t^f_g\right]. \tag{21}$$

Similarly to line faults, if the fault duration is known in advance, this information is included in the optimization problem. As a consequence of a distribution grid fault, the microgrid has to be operated in the island mode, hence relying only on the power that is produced by its renewable generators and energy that is stored in the storage systems.

3) Communication Network Fault: A communication network fault happens if a communication link is physically disconnected or if a cyberattack is detected and communication on that link is no longer reliable. This fault is modeled by modifying the entries of the adjacency matrix $A(t)$ described in Section II-B. In particular, if the communication link among agents i and j is not active, we set

$$a_{i,j}(t) = a_{j,i}(t) = 0. \tag{22}$$

As a consequence, the performance of the energy management algorithm degrades in terms of time required to converge to the solution. In contrast to previous faults, the constraints and objectives of the optimization problem are not modified.

III. Distributed EMS

We propose to design the EMS as an MPC in which the optimization problem that is formulated at each time step is solved via DO combining the advantages of both MPC and DO. On the one hand, MPC can efficiently compensate for uncertainty in the system dynamics, renewable power generation, and energy prices. On the other hand, DO algorithms allow the solution of the optimization problem to be obtained by sharing a limited amount of information and without requiring a central unit. Hereinafter, the DO-based MPC algorithm will be outlined; then, the method to make the algorithm resilient to faults is described.

A. DO-Based MPC

The MPC optimization problem is formulated as a constraint-coupled DO problem [45] as follows:

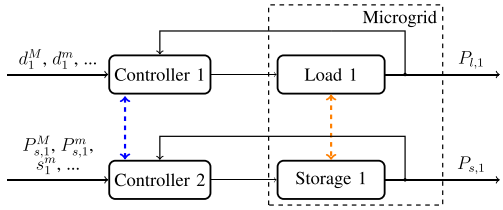

Fig. 1. Example of the controller architecture.

$$2 \min_{\{\mathbf{x}_1, \dots \mathbf{x}_N\}} \quad \sum_{i=1}^{N} f_i(\mathbf{x}_i) \tag{23a}$$

$$\text{s.t.} \quad \mathbf{x}_i \in X_i \tag{23b}$$

$$\sum_{i=1}^{N} \mathbf{g}_i(\mathbf{x}_i) \leq 0 \tag{23c}$$

where x_i is the local decision variable, (23a) is the sum of local objectives f_i, (23b) is the local constraint, and (23c) is the coupling constraint that couples all the local decision variables. An example of the schematic of the controller architecture for a microgrid composed of two agents is shown in Fig. 1. Each microgrid component is equipped with a local controller that coordinates with the other controllers through a communication network (blue line). The physical interconnection between components (buses and lines) is represented by an orange line. The inputs to the local controller are all the information required to formulate the optimization problem (e.g., power limits), and the output is the future power schedule. In this article, the solution of the optimization problem (23a)–(23c) is computed through the distributed algorithm presented in [46]. In brief, this algorithm consists of three steps from the perspective of agent i.

1) Gather the dual variables of the optimization problem from the neighbors.
2) Compute the local primal variable x_i by minimizing the ith part of the Lagrangian.
3) Update the local estimate of the dual variable.

Further details about the algorithm are omitted due to space constraints; the interested reader may refer to [46]. One attractive feature of this algorithm is that it allows the solution to be computed keeping private local information (encoded in x_i, f_i, X_i, and g_i) and sharing only the dual variables that do not have a physical meaning.

The local decision variable $x_i \in \mathbb{R}^T$ of each agent is its future power profile for the next T time steps

$$\mathbf{x}_i(t) = \{P_i(t), \dots P_i(t+T-1)\}. \tag{24}$$

The local objective functions of each agent $f_i : \mathbb{R}^T \to \mathbb{R}$ have been described in Section II. The whole objective is the sum of these local objectives as in (23a)

$$\sum_{i=1}^{N} f_i(\mathbf{x}_i) = \sum_{i=1}^{N_r} J_{r,i} + \sum_{i=1}^{N_l} J_{l,i} + \sum_{i=1}^{N_s} J_{s,i} + \sum_{i=1}^{N_z} J_{z,i} + \sum_{i=1}^{N_g} J_{g,i}. \tag{25}$$

The local constraint set $X_i \subseteq \mathbb{R}^T$ of (23b) includes all the constraints described in Section II for the agents:

1) the maximum produced power at each time step (1) for renewable generators;
2) the maximum and minimum power demand (3) for loads;
3) the system dynamics (5), and the charge and power limits (6), (7) for storage systems;
4) the system dynamics (9), the charge and power limits (10), (11), and the target charge (12) for EVs;
5) the maximum power (14) that is modified by (21) in the case of fault for the external connections.

The coupling constraint (23c) is expressed through the function $g_i : \mathbb{R}^T \to \mathbb{R}^{n_c}$ (where n_c is the number of coupling constraints) for each agent, and it includes constraints (16) and (17). The function g_i has to be specified for each agent and can be written as an affine function of the local decision variable $g_i(x_i) = G_i x_i + h_i$. The formulation of G_i and h_i for each agent is omitted due to space constraints.

Additional constraints required to make the EMS resilient to power grid faults are enforced as local and coupling constraints and will be described in the following.

B. Resilient EMS

In order to make the presented algorithm resilient to the faults described in Section II-C, both the proactive scheduling and outage management strategies are employed.

As described in Section II-C, in the case of a line fault, power cannot flow through that line; hence, there is a risk to overload the other lines of the microgrid. To take the fault into account, constraint (17) is modified into (20) for the faulty line.

In the case of a utility grid fault, power cannot be exchanged with the utility grid through any connection (21). As a consequence, the power cannot be sold in the case of overproduction of the renewable generators and cannot be bought if required by the loads. Hence, a key role is played by agents that can store energy in the microgrid: storage systems and all the EVs provided with V2G technology. Similarly to [30] for the centralized case, we propose to store in such systems enough energy to sustain the microgrid operation until fault recovery. The minimum load energy requirement for the next ν steps is

$$\tilde{r}_\nu(t) = \sum_{i=1}^{N_l} \sum_{\tau=t}^{t+\nu-1} T_s d_i^m(\tau). \tag{26}$$

Hence, in order to guarantee critical load demand and EVs charging, for the next ν steps, we set

$$\sum_{i=1}^{N_s} s_i(t) + \sum_{i=1}^{\tilde{N}_z} \tilde{z}_i(t) \geq \tilde{r}_\nu(t) \quad \forall\, k \in \{t, \dots t+T-1\} \tag{27}$$

where $\tilde{N}_z$ is the subset of EVs provided with V2G technology and $\tilde{z}_i$ is the amount of energy in excess with respect to the target charge z_i^* stored in the vehicle

$$\tilde{z}_i = z_i - z_i^*. \tag{28}$$

Then, setting the target charge $\bar{z}_i$ of objective function (13) to the maximum charge value z_i^M, the EV will try to store an amount of energy greater than its target value z_i^*, hence storing energy that can be supplied to the microgrid if necessary. The choice of the parameter ν has to be done according to the available storage capacity and the estimated time required to recover from a fault (as done for example, in [30]). Clearly, a high value of the ν parameter allows us to deliver power to loads in the case of fault for longer, but it reduces the amount of available storage capacity for the other goals of the storage system, such as peak shaving and valley filling.

Remark 1: Constraint (27) is enforced as a coupling constraint through a suitable definition of local g_i functions in (23c) for each agent. Therefore, this constraint requires neither loads to share their future power demand nor batteries and EVs to share their SoC. Moreover, the constraint corresponding to the utility grid fault (21) is implemented locally as local constraint (23b), hence keeping information about the current fault state private.

As written in Section II-A, battery lifetime can be increased if the battery is not fully drained. However, in some cases, it is tolerable to drain it below the lower limit. Since faults should not happen very often and the fault duration may not be known in advance, we propose to use this amount of energy to cope with faults of unknown duration. In the case of faults, the lower bound of constraint (6) is relaxed as

$$s_i^m - \varepsilon_i \leq s_i(t) \leq s_i^M. \tag{29}$$

A new optimization variable is introduced for each storage system, $\varepsilon_i \in \mathbb{R}$, weighted through the following objective function that is added to (8):

$$J_{\varepsilon_i} = \lambda_i \varepsilon_i. \tag{30}$$

The new variable ε_i is subject to the following constraint:

$$0 \leq \varepsilon_i \leq s_i^m. \tag{31}$$

Depending on the value of the weight λ_i, it is more or less likely to drain a battery below its lower limit.

The optimization problem (23a)–(23c) is reformulated at each time step; hence, the constraints and the cost functions can be modified depending on the current situation. As soon as a fault is detected, the controller is switched to safe mode enabling the constraints presented in this section. This procedure is outlined in Algorithm 1.

IV. Simulation Results

In this section, the results obtained by applying the proposed algorithm to five different simulation scenarios are presented. In scenario 1, we consider the proposed distributed algorithm, without additional constraints and decision variables (presented in Section III-B) required to make it resilient to faults. We show that it allows us to obtain results similar to a centralized approach in a fault-free case. In scenario 2, we illustrate the performance of the resilient algorithm proposed in this article in faulty conditions. In scenario 3, two EVs are included in the microgrid, and we show how the excess energy stored in vehicles can be used to supply power to loads when necessary while meeting the vehicles' charging requirements. In scenario 4, we applied the algorithm to a large-scale microgrid showing that the algorithm is easily scalable and can be applied to LSSs. Finally, scenario 5 shows the performance in case of communication network faults.

Algorithm 1: Distributed Resilient EMS.

For each time step t
input : Comm. network adjacency matrix $A(t)$
Parameter ν in (26)
Local objectives f_i: (2),(4),(8),(13),(15)
Local constraint sets X_i: (1),(3),(5-7),(9), (10-12),(14)
Battery state: $s_i(t)\ \forall i \in N_s$
EVs state: $z_i(t)\ \forall i \in N_z$
Local coupling functions g_i:(16),(17),(27)
output: $\{P_i(t), \dots P_i(t+T-1)\}$ for each agent
ε_i for each battery
if *Line fault = True* ***or*** *Grid fault = True* **then**
  $J_{s,i} \leftarrow J_{s,i} + J_{\varepsilon,i}$
  Introduction of the soft constraint: (6) $\leftarrow$ (29)
  constraint (27) is disabled
  if *Line fault = True* **then**
    $P_{L,i}(\tau) = 0\ \forall\ \tau \in [t, t+T]$
  if *Grid fault = True* **then**
    $P_{g,i}(\tau) = 0\ \forall\ \tau \in [t, t+T]$
if *comm. link between agent i and j is disabled* **then**
  $a_{i,j}(t) = a_{j,i}(t) = 0$
Define x_i, f_i, X_i, g_i for each agent
Solve optimisation problem (23a)-(23c)

TABLE I
NUMERICAL VALUE OF THE MAIN SIMULATION PARAMETERS

Param.	Value	Param.	Value	Param.	Value
T	5	$w_{s,i}$	0	s_i^M	2184 Wh
T_s	1 h	$w_{P_{s,i}}$	0	s_i^m	195 Wh
γ	0.9	w_r	1	$P_{s,i}^M$	500 W
P_g^M	2.1 kW	w_l	1	$\mu_{i,c/d}$	0.98/1.02
P_g^m	–4.2 kW	λ	10	ν	3 h (S.2), 1 h (S.3,4)

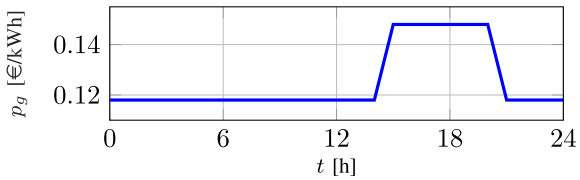

Fig. 2. Electricity price profile [48].

The values of main simulation parameters and energy price profile are presented in Table I and Fig. 2. Simulations are compared using three different indices:

1) produced energy, that is the percentage of energy injected in the grid by each kind of agent;
2) consumed energy, that is the percentage of energy absorbed by each kind of agent;
3) total electricity cost, that is the total cost of the energy bought from the utility grid throughout the simulation, computed as $-\sum_{t=0}^{24}\sum_{i=1}^{N_g} p_g(t)P_{g,i}(t)$.

Simulations were implemented in Python using DISROPT [47] package for DO setting the number of iterations to 1000 and a decreasing step size defined as $\frac{1}{(k+1)^{0.1}}$, where k is the algorithm iteration. The maximum runtime for executing

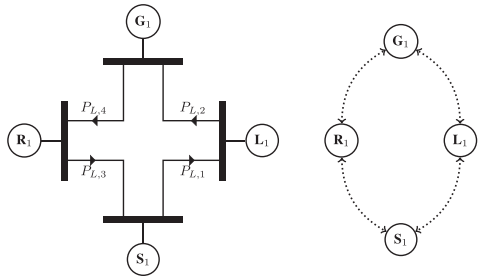

Fig. 3. Four-bus microgrid of [48] and the corresponding communication network.

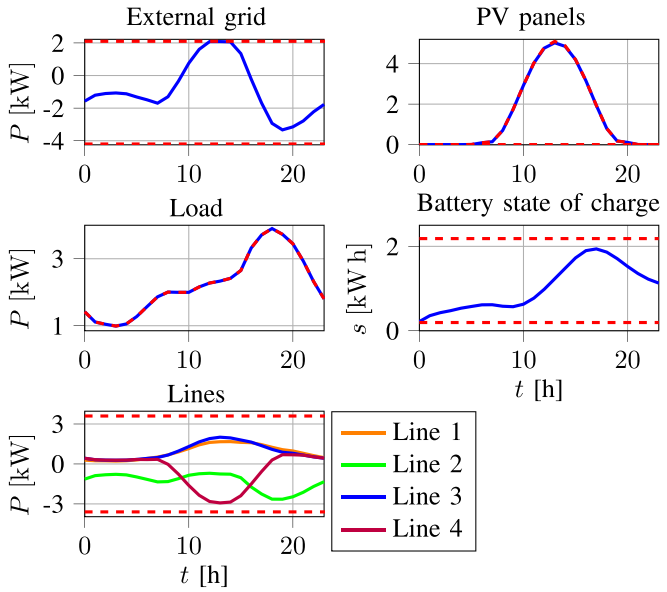

Fig. 4. Power profiles and battery SoC of scenario 1; red-dashed lines represent the power limits. Hereinafter, red-dashed curves denote the lower/upper bounds within which the signals have to stay.

one simulation step is 10 s for scenarios 1, 2, and 3 and 90 s for scenario 4 with an Intel Core$^{\text{TM}}$ i7-2600 CPU @ 3.4 GHz and 16-GB RAM.

Remark 2: Simulation results are influenced by the parameters, in particular the weights, of the objective functions. These are chosen by each agent depending on its priorities and requirements, and given the employed DO algorithm, it is not necessary to share them with the network of agents. Tuning such weights is out of scope for this article; hence, they are kept constant for all the simulation scenarios to allow for a fair comparison.

1) Scenario 1: The first simulation is a comparison with the results presented in [48] to show that the distributed setting proposed in this article obtains results similar to the centralized case. The considered microgrid, presented in Fig. 3, is composed of a renewable generator (PV panels), an energy storage system, a critical load, and a utility grid connection. No faults are simulated, and we are not applying the resilient method described in Section III-B. Simulation results are presented in Fig. 4. In this simulation, the power demand of the critical load is always met, and all the power produced by the renewable generator is used. Between time steps $t = 10$ and $t = 17$, the power produced by

TABLE II
NUMERICAL RESULTS OF SCENARIO 1

Power	Produced [%]	Consumed [%]
P_{ug}	46 (40)	15 (12)
P_{es}	2 (9)	2 (9)
P_{pv}	52 (51)	–
P_{load}	–	82 (79)

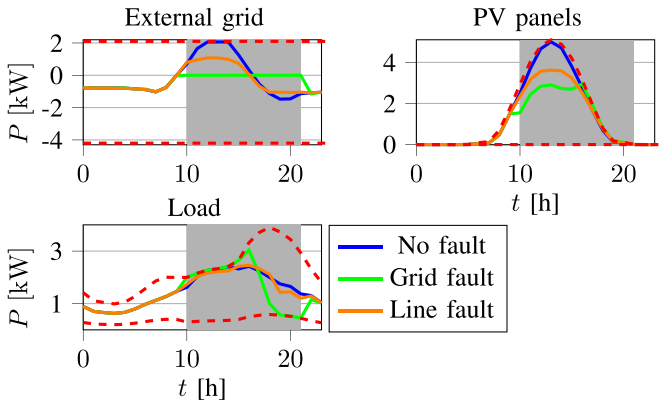

Fig. 5. Power profiles of scenario 2.

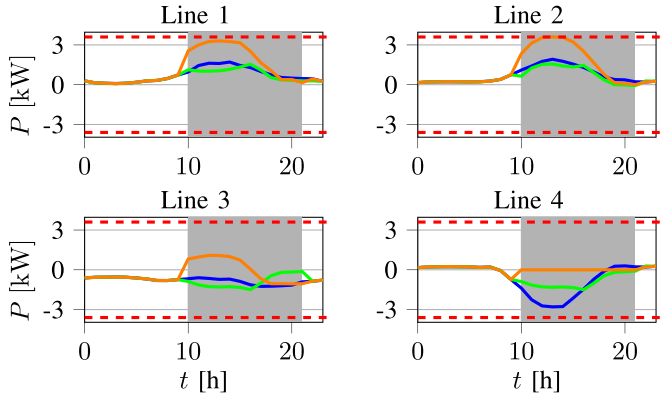

Fig. 6. Line power flows of scenario 2.

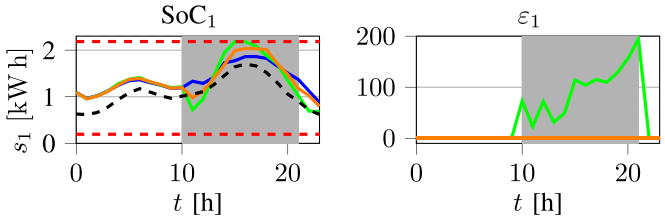

Fig. 7. SoC and ε_1 of scenario 2. The black-dashed line represents the minimum load energy requirement $\tilde{r}_\nu$.

the renewable generator is used to supply the load and charge the battery, and the overproduction is sold to the utility grid (power flow P_g is positive). In the subsequent time steps, the load is supplied by discharging the battery and buying power from the utility grid since the renewable energy production is insufficient. Line power flows are always within their limits, and the peak is at time $t = 13$ where power produced by the PV panels is sold to the utility grid and flows mainly through line 4. Table II contains some numerical results that can be compared with [48, Table 4.4.3] (results of [48] are written in brackets). In particular, Table II shows how the total amount of produced/consumed power (i.e., injected in/drawn from the microgrid) is distributed among the components over the simulation period. Most of the percentages are similar, the main difference being the battery usage. Using the distributed EMS, less power is exchanged with the battery, and this difference is mainly compensated by the utility grid. It follows that the total electricity cost is slightly higher (2.69€ instead of 2.46€).

2) Scenario 2: We apply the proposed resilient EMS to the microgrid of scenario 1. The goal of this simulation scenario is to show the efficacy of our algorithm for energy management purposes under different fault conditions taking into account noncritical loads and constraint (27). The results in Figs. 5–7 refer to three different cases:

1) no faults;
2) utility grid fault;
3) line fault.

All the faults are simulated between time step $t = 10$ and $t = 22$ and are highlighted by a gray background.

The load demand is always met, and the battery SoC is always higher than the minimum load energy requirement for the next ν steps (SoC plot of Fig. 7).

In case 2, a utility grid fault is simulated to show the resilience of the approach. From the left plot of Fig. 5, it is clear that the power exchanged with the utility grid during the fault is zero. This has two main effects: 1) the overproduction of renewable energy cannot be sold to the utility grid and 2) the power cannot be drawn from the grid to be supplied to the load. However, the power demand is met (bottom plot of Fig. 5) thanks to the power supplied by the storage systems, which have stored enough power to sustain the load. The right plot of Fig. 7 shows the ε variable for storage 1. During the fault, this variable takes a value different from zero since the MPC predicts that the battery has to be drained below s_1^m to sustain the load demand. Moreover, since constraint (27) is disabled during faults, the stored energy can be lower than the future power demand of the next ν steps. Hence, in the right plot of Fig. 7, the SoC drops below the $\tilde{r}_\nu$ curve.

In the third case, a fault in line 4 is simulated. In the line 4 plot of Fig. 6, power flow through line 4 is zero during fault; hence, there is a higher power flow through lines 1 and 3. However, these lines are not overloaded thanks to constraint (17). Even though the load demand is always met, the line fault has the effect of reducing the amount of power that is sold to the utility grid, and hence, not all the power produced by the renewable generators is injected in the microgrid.

The results for the three cases are presented in Table III. In the case of a grid fault, the energy exchanged with the grid is lower, and at the same time, more power is exchanged with the batteries.

The total electricity cost in the three cases is:

1) 0.70 € for the no fault case;

TABLE III
NUMERICAL RESULTS OF SCENARIO 2

Power	Produced [%]			Consumed [%]		
Fault	NO	Grid	Line	NO	Grid	Line
P_{ug}	32	27	34	21	0	13
P_{es}	3	7	4	2	6	4
P_{pv}	65	66	34	–	–	–
P_{load}	–	–	–	76	94	83

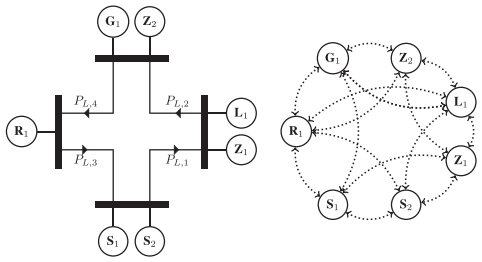

Fig. 8. Four-bus microgrid for simulation scenario 3 and the corresponding communication network.

TABLE IV
EV DATA USED IN SCENARIO 3

Vehicle ID	τ_i^i	τ_i^f	$\bar{z}_i$	V2G
1	8	16	$0.8z_1^M$	yes
2	14	22	$0.9z_2^M$	yes

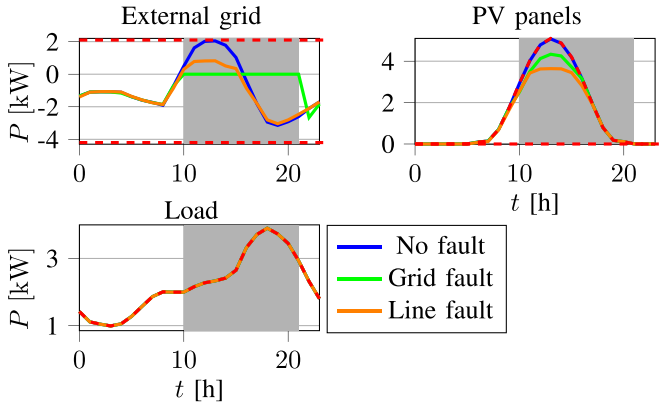

Fig. 9. Power profiles of scenario 3. Similarly to scenario 2, faults are simulated between time steps $t = 10$ and $t = 22$ and highlighted in gray.

2) 1.14 € for the grid fault case;
3) 1.13 € for the line fault case.

3) Scenario 3: In the third scenario, we apply the resilient EMS algorithm to a microgrid that includes a connection to the utility grid, a renewable generator, a critical load, two EVs, and two storage systems, as in Fig. 8. The goal of this simulation is to show that our algorithm is capable of scheduling the charge operation of EVs connected to the microgrid, and that their excess power can be used during faults to meet load demand. The EVs' arrival time, departure time, and target charge are written in Table IV. The other parameters (max charge and max power) are the same used for batteries. We have simulated this system for the same cases considered in scenario 2. The results are plotted in Figs. 9–12. In Fig. 10, the power profiles and SoCs

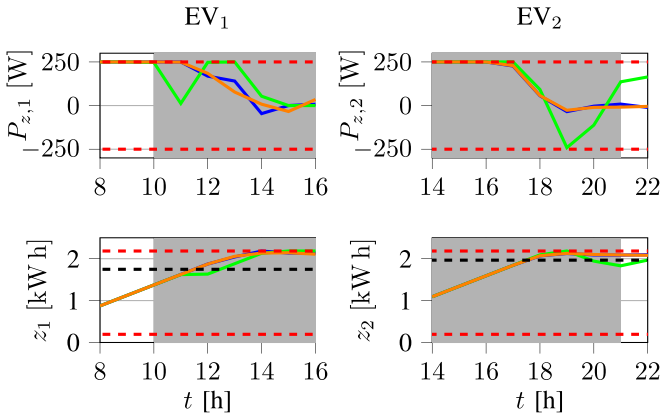

Fig. 10. Power profiles and states of charge of EVs of scenario 3. Black-dashed lines represent the target charge $\bar{z}_i$ of each vehicle.

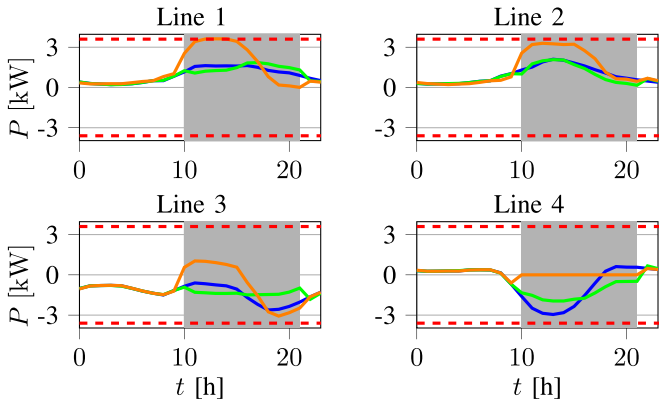

Fig. 11. Line power flows of scenario 3.

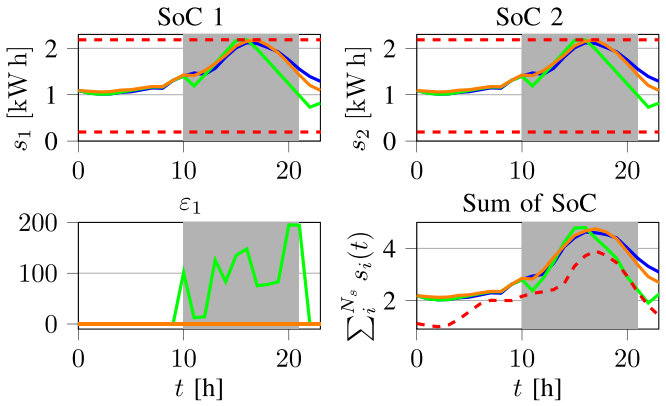

Fig. 12. SoCs, ε, and sum of stored energy of scenario 3. Red-dashed lines represent the limits of SoC and sum of SoC.

of the EVs are shown only for the time steps when the vehicles are parked. In the first case (no faults), all the power produced by the PV panels is injected into the microgrid, and the load power demand is met (see Fig. 9). Both of the EVs achieve their target SoC without exceeding the maximum power limit (see Fig. 10). The algorithm ensures that the sum of the battery charge and the available EVs' stored energy is always higher than the future

TABLE V
NUMERICAL RESULTS OF SCENARIO 3

Power	Produced [%]			Consumed [%]		
Fault	NO	Grid	Line	NO	Grid	Line
P_{ug}	46	34	51	14	0	6
P_{es}	2	3	2	2	3	2
P_{pv}	52	62	47	–	–	–
P_{load}	–	–	–	82	95	90
P_z	0	1	0	2	2	2

power demand, hence guaranteeing that the load demand is met for the next ν steps.

In the second case (grid fault), power cannot be exchanged with the utility grid during the fault (first plot of Fig. 9). As a consequence, not all the power produced by the PV panels can be injected in the microgrid; however, load demand is met. During the fault, power has to be provided to the load by the other components, in particular PV panels, batteries, and EVs. EV_2 has to supply power to the microgrid between time steps $t = 18$ and $t = 20$ (power is negative in this time period in Fig. 10). The vehicle charge drops below its target charge at time step $t = 21$ (z_2 plot of Fig. 10). However, at the next time step (which corresponds to the vehicle departure time), it is again above the target value. Fig. 12 shows that the ε_1 variable takes values different from zero. This is due to the fact that the controller predicts that in the case of a persistent fault, the battery has to be depleted below its lower limit to sustain the power demand. The total available energy is always greater than the future power requirement (sum of the SoC plot of Fig. 12), hence ensuring to meet load demand for the next ν steps. However, between time steps $t = 18$ and $t = 22$, when load demand is high and PV panels do not produce high amount of power, the green line lays on its minimum value.

In the third case (line fault), power cannot flow over line 4 causing a higher power flow through the other lines. It is clear from Fig. 9 that the load power demand is always met; however, not all the power produced by the PV panels can be injected in the utility grid. Comparing the left plot of Fig. 9 and the top left plot of Fig. 11, it is clear that PV power injection is reduced not to overload line 1. The target charge of both the EVs is reached before their departure, and it is not necessary to discharge the vehicles to supply the loads.

Table V shows numerical results. The total electricity cost in the three cases is:

1) 2.87 € for the no fault case;
2) 2.07 € for the grid fault case;
3) 3.54 € for the line fault case.

4) Scenario 4: We apply the proposed algorithm to the microgrid in Fig. 13. The architecture is composed of 31 agents and 40 lines (in Fig. 13, only the first two and the last unit are represented). All the parameters of the agents (e.g., max power flow, max storage capacity, etc.) are the same as in scenario 1 except the MPC prediction horizon T (which is set to 10 to increase the number of decision variables and constraints of the optimization problem to show that the algorithm is suitable for LSSs), the limits on power that can be exchanged with the utility grid (which have been increased by a factor 10), and the load

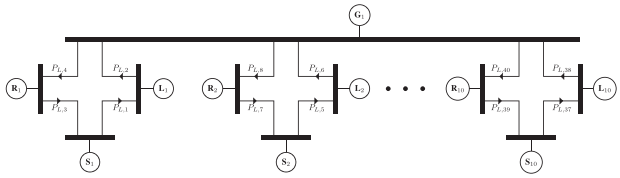

Fig. 13. Large-scale microgrid used for simulation scenario 4.

TABLE VI
NUMERICAL RESULTS OF SCENARIO 4

Power	Produced [%]	Consumed [%]
P_{ug}	40	0
P_{es}	4	3
P_{pv}	56	–
P_{load}	–	97

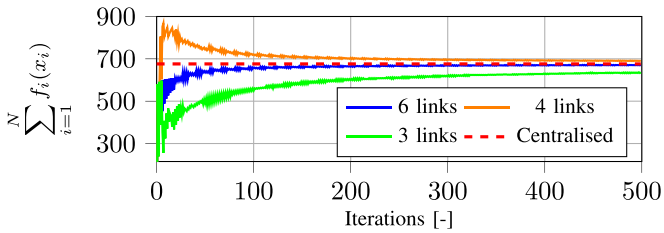

Fig. 14. Convergence of the distributed cost to the centralized one with a different number of enabled communication links.

power demand profile of five out of ten loads (which has been set as the commercial load profile of [48]). For this simulation, agents are allowed to communicate using 60% of all possible "all-to-all" graph links, i.e., 279 out of 465.

In this setting, at each time step, the controllers compute 310 decision variables subject to 950 local constraints and 830 coupling constraints. However, since the computation is spread among all the agents of the microgrid, the computational power expended by each agent does not change with respect to the previous cases. The simulation results are presented in Table VI; the total electricity cost is 24.70 €.

5) Scenario 5: We investigate the algorithm's performance when errors or attacks are present in the communication network and some communication links cannot be used. Since the presented algorithm is distributed, the communication network plays a key role in the algorithm performance, in particular in the convergence time of the algorithm. Since the problem is convex, the optimization problem has a unique optimal solution; hence, the DO algorithm employed in this article [46] guarantees convergence to the solution of the centralized optimization problem even if each node is not communicating with all the others, as long as the communication graph remains connected. Hence, we simulated the first step of scenario 1 ($t = 0$) under different communication network conditions.

1) Case 1: six out of six communication links are enabled.
2) Case 2: four out of six communication links are enabled.
3) Case 3: three out of six communication links are enabled.

Fig. 14 shows the convergence of the sum of local costs in (25) to the centralized cost over the algorithm iterations in the three

different cases. It is clear that increasing the number of communication links decreases the time required to the distributed algorithm to converge to the optimal cost while enforcing the coupling constraints.

V. Conclusion

In this article, we present a novel distributed MPC algorithm suitable for microgrid energy management. The optimization problem that is formulated at each time step is solved using a DO algorithm that preserves privacy. Since all computations are performed locally by each agent relying only on local information and exchanging data only with neighbors, the resulting architecture is fully distributed, and each node requires only limited computational power. The proposed algorithm has first been compared with a centralized approach and has been shown to obtain similar results. In order to make the algorithm resilient to faults in the microgrid system, we enforced additional constraints and decision variables to the optimization problem, so that minimum load demand is guaranteed for some time steps in fault conditions without overloading the lines. Moreover, the proposed EMS is suitable to compute the charge scheduling of EVs connected in the microgrid integrating their goals with those of other microgrid agents. The excess of charge of EVs can be used to supply energy to the microgrid in the case of necessity, hence increasing the resilience of the system. Finally, we show that, thanks to the specific optimization algorithm that has been employed, the distributed controller is resilient to faults in the communication network. As a future work, we plan to overcome the main limitations of the proposed method. First of all, we will consider different types of faults and even attacks in the controller. The detection problem and the estimation of the future profiles of renewable power generators, loads, and electricity price are also the topics of future study.

References

[1] R. Lasseter, "Microgrids," in *Proc. IEEE Power Eng. Soc. Winter Meeting*, 2002, vol. 1, pp. 305–308.

[2] D. E. Olivares et al., "Trends in microgrid control," *IEEE Trans. Smart Grid*, vol. 5, no. 4, pp. 1905–1919, Jul. 2014, doi: 10.1109/TSG.2013.2295514.

[3] S. Ullah, A. M. Haidar, P. Hoole, H. Zen, and T. Ahfock, "The current state of distributed renewable generation, challenges of interconnection and opportunities for energy conversion based DC microgrids," *J. Cleaner Prod.*, vol. 273, 2020, Art. no. 122777.

[4] Y. Yoldaş, A. Önen, S. Muyeen, A. V. Vasilakos, and İ. Alan, "Enhancing smart grid with microgrids: Challenges and opportunities," *Renewable Sustain. Energy Rev.*, vol. 72, pp. 205–214, 2017.

[5] A. Hussain, V.-H. Bui, and H.-M. Kim, "A resilient and privacy-preserving energy management strategy for networked microgrids," *IEEE Trans. Smart Grid*, vol. 9, no. 3, pp. 2127–2139, May 2018.

[6] T. W. Mak, F. Fioretto, L. Shi, and P. Van Hentenryck, "Privacy-preserving power system obfuscation: A bilevel optimization approach," *IEEE Trans. Power Syst.*, vol. 35, no. 2, pp. 1627–1637, Mar. 2019.

[7] C. Colson and M. Nehrir, "A review of challenges to real-time power management of microgrids," in *Proc. IEEE Power Energy Soc. Gen. Meeting*, 2009, pp. 1–8.

[8] W. Gu, Z. Wu, and X. Yuan, "Microgrid economic optimal operation of the combined heat and power system with renewable energy," in *Proc. IEEE Power Energy Soc. Gen. Meeting*, 2010, pp. 1–6.

[9] I. Prodan and E. Zio, "A model predictive control framework for reliable microgrid energy management," *Int. J. Elect. Power Energy Syst.*, vol. 61, 2014, pp. 399–409.

[10] A. Parisio, E. Rikos, and L. Glielmo, "A model predictive control approach to microgrid operation optimization," *IEEE Trans. Control Syst. Technol.*, vol. 22, no. 5, pp. 1813–1827, Sep. 2014.

[11] Y. Guo, J. Xiong, S. Xu, and W. Su, "Two-stage economic operation of microgrid-like electric vehicle parking deck," *IEEE Trans. Smart Grid*, vol. 7, no. 3, pp. 1703–1712, May 2016.

[12] S. R. Cominesi, M. Farina, L. Giulioni, B. Picasso, and R. Scattolini, "A two-layer stochastic model predictive control scheme for microgrids," *IEEE Trans. Control Syst. Technol.*, vol. 26, no. 1, pp. 1–13, Jan. 2018.

[13] C. A. Hans, P. Sopasakis, A. Bemporad, J. Raisch, and C. Reincke-Collon, "Scenario-based model predictive operation control of islanded microgrids," in *Proc. IEEE 54th Conf. Decis. Control*, 2015, pp. 3272–3277.

[14] S. Habib, M. Kamran, and U. Rashid, "Impact analysis of vehicle-to-grid technology and charging strategies of electric vehicles on distribution networks—A review," *J. Power Sources*, vol. 277, pp. 205–214, 2015, doi: 10.1016/j.jpowsour.2014.12.020.

[15] B. Wang et al., "Predictive scheduling for electric vehicles considering uncertainty of load and user behaviors," in *Proc. IEEE/PES Transmiss. Distrib. Conf. Expo.*, 2016, pp. 1–5.

[16] U. Ur Rehman, K. Yaqoob, and M. A. Khan, "Optimal power management framework for smart homes using electric vehicles and energy storage," *Int. J. Elect. Power Energy Syst.*, vol. 134, 2022, Art. no. 107358.

[17] H. Pourbabak, Q. Alsafasfeh, and W. Su, "A distributed consensus-based algorithm for optimal power flow in dc distribution grids," *IEEE Trans. Power Syst.*, vol. 35, no. 5, pp. 3506–3515, Sep. 2020.

[18] Y. Zheng, S. Li, and R. Tan, "Distributed model predictive control for on-connected microgrid power management," *IEEE Trans. Control Syst. Technol.*, vol. 26, no. 3, pp. 1028–1039, May 2017.

[19] A. Parisio, C. Wiezorek, T. Kyntäjä, J. Elo, K. Strunz, and K. H. Johansson, "Cooperative MPC-based energy management for networked microgrids," *IEEE Trans. Smart Grid*, vol. 8, no. 6, pp. 3066–3074, Nov. 2017.

[20] P. Braun, T. Faulwasser, L. Grüne, C. M. Kellett, S. R. Weller, and K. Worthmann, "Hierarchical distributed ADMM for predictive control with applications in power networks," *IFAC J. Syst. Control*, vol. 3, pp. 10–22, 2018.

[21] I. Notarnicola and G. Notarstefano, "Constraint-coupled distributed optimization: A relaxation and duality approach," *IEEE Trans. Control Netw. Syst.*, vol. 7, no. 1, pp. 483–492, Mar. 2020.

[22] C. L. Prete et al., "Sustainability and reliability assessment of microgrids in a regional electricity market," *Energy*, vol. 41, no. 1, pp. 192–202, 2012.

[23] A. Hussain, V.-H. Bui, and H.-M. Kim, "Microgrids as a resilience resource and strategies used by microgrids for enhancing resilience," *Appl. Energy*, vol. 240, pp. 56–72, 2019.

[24] J.-J. Prince A., P. Haessig, R. Bourdais, and H. Guéguen, "Resilience in energy management system: A study case," *IFAC-PapersOnLine*, vol. 52, no. 4, pp. 395–400, 2019.

[25] N. S. Raman, N. Gaikwad, P. Barooah, and S. P. Meyn, "Reinforcement learning-based home energy management system for resiliency," in *Proc. Amer. Control Conf.*, 2021, pp. 1358–1364.

[26] J. Marquez, A. Zafra-Cabeza, C. Bordons, and M. A. Ridao, "A fault detection and reconfiguration approach for MPC-based energy management in an experimental microgrid," *Control Eng. Pract.*, vol. 107, 2021, Art. no. 104695.

[27] E. Bernardi, M. M. Morato, P. R. Mendes, J. E. Normey-Rico, and E. J. Adam, "Fault-tolerant energy management for an industrial microgrid: A compact optimization method," *Int. J. Elect. Power Energy Syst.*, vol. 124, 2021, Art. no. 106342.

[28] H. Ghasemieh, B. R. Haverkort, M. R. Jongerden, and A. Remke, "Energy resilience modelling for smart houses," in *Proc. 45th Annu. IEEE/IFIP Int. Conf. Dependable Syst. Netw.*, 2015, pp. 275–286.

[29] M. R. Jongerden, J. Hüls, A. Remke, and B. R. Haverkort, "Does your domestic photovoltaic energy system survive grid outages?," *Energies*, vol. 9, no. 9, 2016, Art. no. 736.

[30] I. Prodan, E. Zio, and F. Stoican, "Fault tolerant predictive control design for reliable microgrid energy management under uncertainties," *Energy*, vol. 91, pp. 20–34, 2015.

[31] J. Tobajas, F. Garcia-Torres, P. Roncero-Sánchez, J. Vázquez, L. Bellatreche, and E. Nieto, "Resilience-oriented schedule of microgrids with hybrid energy storage system using model predictive control," *Appl. Energy*, vol. 306, 2022, Art. no. 118092.

[32] R. Roche, F. Berthold, F. Gao, F. Wang, A. Ravey, and S. Williamson, "A model and strategy to improve smart home energy resilience during outages using vehicle-to-home," in *Proc. IEEE Int. Electr. Veh. Conf.*, 2014, pp. 1–6.

[33] Y. Yang and S. Wang, "Resilient residential energy management with vehicle-to-home and photovoltaic uncertainty," *Int. J. Elect. Power Energy Syst.*, vol. 132, 2021, Art. no. 107206.
[34] V. Casagrande, I. Prodan, S. K. Spurgeon, and F. Boem, "A robust MPC method for microgrid energy management based on distributed optimization," in *Proc. Eur. Control Conf.*, 2021, pp. 1963–1968.
[35] H. Zhou, T. Bhattacharya, D. Tran, T. S. T. Siew, and A. M. Khambadkone, "Composite energy storage system involving battery and ultracapacitor with dynamic energy management in microgrid applications," *IEEE Trans. Power Electron.*, vol. 26, no. 3, pp. 923–930, Mar. 2011.
[36] M. Faisal, M. A. Hannan, P. J. Ker, A. Hussain, M. B. Mansor, and F. Blaabjerg, "Review of energy storage system technologies in microgrid applications: Issues and challenges," *IEEE Access*, vol. 6, pp. 35143–35164, 2018.
[37] H. L. Ferreira, R. Garde, G. Fulli, W. Kling, and J. P. Lopes, "Characterisation of electrical energy storage technologies," *Energy*, vol. 53, pp. 288–298, 2013.
[38] R. Dufo-López, J. L. Bernal-Agustín, and J. A. Domínguez-Navarro, "Generation management using batteries in wind farms: Economical and technical analysis for Spain," *Energy Policy*, vol. 37, no. 1, pp. 126–139, 2009.
[39] H. Bindner, T. Cronin, and P. Lundsager, J. F. Manwell, U. Abdulwahid, and I. Baring-Gould, "Lifetime modelling of lead acid batteries," *Benchmarking*, vol. 12, p. 82, 2005.
[40] S. Das, P. Acharjee, and A. Bhattacharya, "Charging scheduling of electric vehicle incorporating grid-to-vehicle (G2V) and vehicle-to-grid (V2G) technology in smart-grid," in *Proc. IEEE Int. Conf. Power Electron. Smart Grid Renewable Energy*, 2020, pp. 1–6.
[41] E. A. Grunditz and T. Thiringer, "Performance analysis of current BEVs based on a comprehensive review of specifications," *IEEE Trans. Transp. Electrific.*, vol. 2, no. 3, pp. 270–289, Sep. 2016.
[42] S. Stüdli, E. Crisostomi, R. Middleton, and R. Shorten, "Optimal real-time distributed V2G and G2V management of electric vehicles," *Int. J. Control*, vol. 87, pp. 1153–1162, 2014, doi: 10.1080/00207179.2013.868930.
[43] C. Kiebler, I. Prodan, F. Petzke, and S. Streif, "Reserve balancing in a microgrid system for safety analysis," *IFAC-PapersOnLine*, vol. 53, no. 2, pp. 13581–13586, 2020.
[44] H. Seifi and M. S. Sepasian, *Electric Power System Planning: Issues, Algorithms and Solutions*, New York, NY, USA: Springer, 2011.
[45] G. Notarstefano et al., "Distributed optimization for smart cyber-physical networks," *Found. Trends Syst. Control*, vol. 7, no. 3, 2019, pp. 253–383.
[46] A. Falsone, K. Margellos, S. Garatti, and M. Prandini, "Dual decomposition for multi-agent distributed optimization with coupling constraints," *Automatica*, vol. 84, pp. 149–158, 2017.
[47] F. Farina, A. Camisa, A. Testa, I. Notarnicola, and G. Notarstefano, "DISROPT: A Python framework for distributed optimization," *IFAC-PapersOnLine*, vol. 53, no. 2, pp. 2666–2671, 2020.
[48] I. Zafeiratou, "Hierarchical control of a meshed dc microgrid through constrained optimization," Ph.D. dissertation, Université Grenoble Alpes, Grenoble, France, 2020.

Vittorio Casagrande received the B.Sc. degree in industrial engineering and the M.Sc. degree (*cum laude*) in electrical energy and systems engineering from the University of Trieste, Trieste, Italy, in 2016 and 2019, respectively, and the Ph.D. degree in control engineering from University College London, London, U.K., in 2019.

From September 2017 to February 2018, he was an Erasmus Student with the Eindhoven University of Technology, Eindhoven, The Netherlands. From June 2018 to January 2019, he has been an Intern with Danieli Automation S.p.A., Buttrio, Italy. He has a five-month experience as a Research Associate with the University of Trieste working on machine learning methods for pattern recognition. His current research interests include energy management for microgrid systems, distributed fault-tolerant control, and cyber-physical systems.

Ionela Prodan received the B.S. degree in automation and applied informatics from the Politehnica University of Bucharest, Bucharest, Romania, in 2009, and the Ph.D. degree in control engineering from Supélec, Gif-sur-Yvette, France, in 2012.

She continued with a Postdoctoral Fellowship within the Chair on Systems Science and the Energetic Challenge—EDF, École Centrale Paris, France. Since 2014, she has been an Associated Professor with the Laboratory of Conception and Integration of Systems, Université Grenoble Alpes, Valence, France. She obtained her Habilitation to Conduct Research (HDR) in 2020. Her research interests are multidisciplinary with a core expertise in control and applied mathematics, encompassing constrained optimization-based control (model-predictive control via distributed and decentralized approaches), mixed-integer programming, differential flatness, set-theoretic methods, and their application to motion planning for autonomous vehicles and energy management in building-scale microgrids.

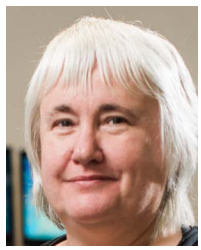

Sarah K. Spurgeon (Fellow, IEEE) received the B.Sc. degree in mathematics and D.Phil. degree in electronics from the University of York, York, U.K., in 1985 and 1988, respectively.

She has held previous academic positions with the University of Loughborough, Loughborough, U.K., the University of Leicester, Leicester, U.K., and the University of Kent, Canterbury, U.K. He is currently a Professor of Control Engineering and the Head of the Department of Electronic and Electrical Engineering, University College London, London, U.K. She has authored or coauthored more than 300 research papers in her research areas. Her research interests include system modeling and analysis, robust control, and estimation.

Dr. Spurgeon was the recipient of the Honeywell International Medal for "distinguished contribution as a control and measurement technologist to developing the theory of control" in 2010 and an IEEE Millennium Medal in 2000. She is an Editor-in-Chief for IEEE Press and the Vice-President Publications of the International Federation of Automatic Control.

Francesca Boem (Member, IEEE) received the M.Sc. degree (*cum laude*) in management engineering and the Ph.D. degree in information engineering from the University of Trieste, Trieste, Italy, in 2009 and 2013, respectively.

From 2013 to 2014, she was a Postdoctoral Researcher with the Machine Learning Group, University of Trieste. From 2014 to 2018, she was a Research Associate with the Department of Electrical and Electronic Engineering, Imperial College London, London, U.K. Since 2015, she has been part of the team with Imperial College London working on the flagship EU H2020-WIDESPREAD-TEAMING project for the development of the EU KIOS Research and Innovation Centre of Excellence. In 2018, she joined the Department of Electronic and Electrical Engineering, University College London, as a Lecturer. Her current research interests include distributed fault diagnosis and fault-tolerant control methods for large-scale networked systems, safety and security of cyber-physical systems, and learning-based control.

Dr. Boem is a Member of the International Federation of Automatic Control (IFAC) Technical Committee 6.4 ("Fault Detection, Supervision and Safety of Technical Processes–SAFEPROCESS") and an Associate Editor for IEEE SYSTEMS JOURNAL, for the IEEE Control System Society Conference Editorial Board, and for the European Control Association (EUCA) Conference Editorial Board. She is a Publicity Chair for 2022 IFAC/EUCA European Control Conference.